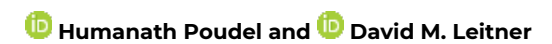
# Locating dynamic contributions to allostery via determining rates of vibrational energy transfer

Cite as: J. Chem. Phys. 158, 015101 (2023); https://doi.org/10.1063/5.0132089

Submitted: 26 October 2022 • Accepted: 09 December 2022 • Accepted Manuscript Online: 09

December 2022 • Published Online: 04 January 2023









#### ARTICLES YOU MAY BE INTERESTED IN

Time-resolved spectroscopic mapping of vibrational energy flow in proteins: Understanding thermal diffusion at the nanoscale

The Journal of Chemical Physics 157, 240901 (2022); https://doi.org/10.1063/5.0116734

Computing chemical potentials of solutions from structure factors

The Journal of Chemical Physics 157, 121101 (2022); https://doi.org/10.1063/5.0107059

Nuclear wave-packet-propagation-based study of the electron-coupled, proton-transfer process in the charge-transfer state of FHCI exhibiting three electronic states in full-dimensional space

The Journal of Chemical Physics 158, 014302 (2023); https://doi.org/10.1063/5.0131104

The Journal of Chemical Physics Special Topics Open for Submissions



## Locating dynamic contributions to allostery via determining rates of vibrational energy transfer

Cite as: J. Chem. Phys. 158, 015101 (2023); doi: 10.1063/5.0132089 Submitted: 26 October 2022 • Accepted: 9 December 2022 • Published Online: 4 January 2023







Humanath Poudel David M. Leitner David M. Leitner





#### **AFFILIATIONS**

Department of Chemistry, University of Nevada, Reno, Nevada 89557, USA

Note: This paper is part of the JCP Special Topic on New Views of Allostery. a) Author to whom correspondence should be addressed: dml@unr.edu

#### **ABSTRACT**

Determining rates of energy transfer across non-covalent contacts for different states of a protein can provide information about dynamic and associated entropy changes during transitions between states. We investigate the relationship between rates of energy transfer across polar and nonpolar contacts and contact dynamics for the β<sub>2</sub>-adrenergic receptor, a rhodopsin-like G-protein coupled receptor, in an antagonist-bound inactive state and agonist-bound active state. From structures sampled during molecular dynamics (MD) simulations, we find the active state to have, on average, a lower packing density, corresponding to generally more flexibility and greater entropy than the inactive state. Energy exchange networks (EENs) are computed for the inactive and active states from the results of the MD simulations. From the EENs, changes in the rates of energy transfer across polar and nonpolar contacts are found for contacts that remain largely intact during activation. Change in dynamics of the contact, and entropy associated with the dynamics, can be estimated from the change in rates of energy transfer across the contacts. Measurement of change in the rates of energy transfer before and after the transition between states thereby provides information about dynamic contributions to activation and allostery.

Published under an exclusive license by AIP Publishing. https://doi.org/10.1063/5.0132089

#### I. INTRODUCTION

The role of protein and water dynamics in the allosteric regulation of structured proteins has long been appreciated and continues to be investigated. 1-15 Well-studied examples, such as G-proteincoupled receptors (GPCRs) and hemoglobins, 16-23 underscore the contributions of protein and water dynamics. Nuclear magnetic resonance (NMR) measurements have provided important information about changes in dynamics that occur with ligand binding from which entropic contributions can be estimated. 24-26 Timeresolved vibrational spectroscopy, currently measuring rates of vibrational energy transfer and pathways through proteins,2 provide a means for further insight into contributions of dynamics to allostery, as both protein structure and dynamics mediate vibrational energy transfer. 17,36-40 In this article, we examine the relationship between change in rates of vibrational energy transfer across polar and nonpolar contacts and contact dynamics during protein activation, specifically of  $\beta_2$ -adrenergic receptor ( $\beta_2AR$ ), a rhodopsin-like GPCR. While past work has emphasized connections between vibrational energy flow and structural change in activation

of β<sub>2</sub>AR, <sup>41</sup> we discuss here how determining rates of energy transfer across polar and nonpolar contacts of β<sub>2</sub>AR in inactive and active states also provides information about changes in contact dynamics and associated entropy with change in the state of the protein.

Even in the absence of structural change, cooperative binding can occur with change in vibrational dynamics upon ligand binding, as discussed by Cooper and Dryden,<sup>42</sup> in which case free energy differences for a sequence of transitions, such as binding ligands, correspond to changes in vibrational entropy. If the structure remains largely unchanged but the packing density of the protein varies slightly with a change in state, there may be a shift in the vibrational frequencies of the protein leading to a change in entropy, which can be estimated in terms of the vibrational mode Grüneisen parameters.<sup>43</sup> Grüneisen parameters quantify how vibrational frequencies change with a change in volume.

Both structural and dynamic changes occur when an agonist binds to  $\beta_2 AR$ .<sup>8</sup> Active states of  $\beta_2 AR$  have been found to be more flexible than inactive states,8 and although there are differences in the overall structures of these states, the greater flexibility of the active state may also be associated with a slightly greater average volume and correspondingly lower packing density. We examine that possibility here, computing volumes of  $\beta_2AR$  in inactive and active states from structures sampled in molecular dynamics (MD) simulations. The on-average smaller packing density that is found for the active state is consistent with its greater flexibility. We use that information to estimate the change in entropy for the transition from an antagonist-bound inactive to active state.

β<sub>2</sub>AR is a well-studied class A GPCR;<sup>8</sup> its structure has been characterized for some time, and it plays an important functional role as a neurotransmitter receptor. 44 We have studied vibrational energy transport in this protein<sup>41</sup> by computing energy exchange networks (EENs) using an approach developed by Yamato and co-workers, 45 where energy currents between residue pairs are computed in terms of energy flux time correlation functions using data from MD simulations. From the EENs, we identified changes in pathways for energy transport due to structural changes of the protein during activation. Because change in EENs is related, at least in part, to change in structure, there are some similarities between maps of the change in EENs and changes in protein contact networks of  $\beta_2AR$  for the transition from inactive to active states.<sup>46</sup> However, there are also differences, as changes in EENs can occur where non-covalent contacts remain intact during activation, but there are changes in the dynamics of the contact. We address this topic here.

We examine how change in rates of energy transfer across polar and nonpolar contacts arises from dynamic changes of the contacts, in addition to the structural changes previously<sup>41</sup> identified, which occur during activation of  $\beta_2 AR$ . We show how the dynamic changes, and their associated change in entropy, can be related to the change in rates of energy transfer for contacts that remain largely intact during activation. Striking dynamic changes during activation of β<sub>2</sub>AR are seen to occur at nonpolar contacts. Even if rates of energy transfer across nonpolar contacts are often small compared with rates across polar contacts,<sup>36</sup> change in rate with change in the functional state of the protein is often found to be sizable, reflecting the change in dynamics of the contact. We expect the relationship between change in rates of energy transfer across the contact and the change in contact dynamics to be useful since rates of energy transfer across non-covalent contacts are currently being measured by time-resolved vibrational spectroscopic techniques.<sup>27-35</sup> We note that many of the measured rates have been reported for energy transfer across nonpolar contacts.28

In Sec. II, we summarize the theoretical and computational methods used for the study of energy transfer across polar and non-polar contacts of  $\beta_2AR$  and the relationship to changes in protein dynamics and entropy. In Sec. III, we present the results for change in the average volume of  $\beta_2AR$  with activation, change in dynamics of polar and nonpolar contacts that remain intact, and the relationship to changes in rates of energy transfer across the contacts. Concluding remarks appear in Sec. IV.

## II. THEORETICAL AND COMPUTATIONAL METHODS A. Computational methods for $\beta_2AR$

The computational study was performed using the initial  $\beta_2AR$  structures from the protein data bank (PDB) entry  $3P0G^{47}$  for the

active state with agonist ligand [BI-167107 ( $C_{21}H_{26}N_2O_4$ )] and PDB entry 2RH1<sup>48</sup> for the inactive state with antagonist ligand [Carazolol ( $C_{18}H_{22}N_2O_2$ )]. The T4-lysozyme chimera of the inactive state was omitted, the missing intercellular loop (ICL3) was modeled using Modeller9.23,<sup>49</sup> and residues 1–28, in the extracellular region, were omitted for both states since they are not resolved in PDB 2RH1 and do not contribute to the properties we study. Missing residues of ICL3 of the active state were modeled using Modeller9.23, providing the same homology for both states.

The modeled structures were uploaded to the CHARMM-GUI<sup>50</sup> online interface in which each was set up in a rectangular box embedded with 170 1-palmitoyl-2-oleoyl-sn-glycero-3phosphocholine (POPC) lipid molecules to model the cell membrane. The systems were solvated with TIP3P<sup>51</sup> waters and neutralized with Na<sup>+</sup> and Cl<sup>-</sup> ions with a final concentration of 0.15 M NaCl. The molecular dynamics (MD) simulations were performed using the AMBER16 MD software package. The AMBER ff14SB<sup>52</sup> forcefield for protein and the Lipid17<sup>53</sup> forcefield for lipids were employed. Each was energy minimized 20 000 steps, in which the first 10 000 steps were carried out using the steepest descent method and the remaining, using the conjugant gradient method. All simulations were performed under periodic boundary conditions. The systems were heated to 300 K from 0.1 K for a ns and kept constant at 300 K for an additional ns. The heating was performed using the Berendsen thermostat<sup>54</sup> in a canonical ensemble. The equilibration simulations were performed under an isothermal-isobaric ensemble applying positional restraint in the protein backbone atoms for 10 ns with a force constant of 1 kcal/(mol Å<sup>2</sup>) and another 20 ns without any positional restraints. The SHAKE algorithm was employed to constrain all bonds containing hydrogen. For  $\beta_2$ AR, production simulations were performed for 100 ns using an isothermal-isobaric (NPT) ensemble. In the NPT simulations, the restart files were saved every ns for the next microcanonical (NVE)

The volume of  $\beta_2AR$  in active and inactive states was estimated using the Protein Volume Program 1.3 developed by Chen and Makhatadze, 55 where default settings have been used. For the volume calculation, 20 structures of  $\beta_2AR$  in each state were taken during the last 50 ns of the MD simulations at equally spaced time intervals. The volume computed for the protein represents the molecular surface volume, which is the total van der Waals volume and the intramolecular void volume. The change in the volume indicates the change in void volume in the activation of the protein. We compute the volume of both states with and without the agonist and antagonist ligands. Our focus is mainly on the latter as there are differences in the size of the ligands, and our interest is the change in the volume and packing density of the protein.

Structures of some of the contacts discussed in this study were examined using clustering analysis of the residue pairs to determine the extent of variation during the last 50 ns trajectory. For this analysis, 2500 structures were used for each state with a neighbor root-mean-square deviation (RMSD) cutoff of 0.2 nm.

To compute the energy currents between residue pairs from the results of the MD simulations, we followed a similar protocol from a prior study. <sup>41</sup> In total, 50 microcanonical (NVE) simulations were performed for each state from the trajectories saved in the prior 100 ns NPT simulations, taking a frame every ns from the 50–100 ns region. Each NVE simulation was carried out for 150 ps

with an integration time of 0.5 fs. Coordinates were saved every 5 fs, and velocities were saved every 1 fs; the average of 5 fs was computed to correspond to the coordinates saved. An Ewald sum tolerance of 10<sup>-7</sup> was applied to reduce the energy drift. Many approaches have been developed to compute energy transport in proteins. <sup>37,56-68</sup> Energy Exchange Networks, EENs, computed using the CUrrent calculation for Proteins (CURP) version 1.2.1 developed by Yamato and co-workers, <sup>45</sup> are convenient for this study since rates of energy transfer and contact dynamics can be computed using the same trajectory. A total of 50 CURP calculations were performed, and a statistical average was computed for each state to compute EENs.

The methodology of CURP, developed by Yamato and coworkers,  $^{45,69,70}$  has been detailed previously.  $^{45,71}$  Briefly, the energy current is obtained from energy flux time correlation functions. The energy flux,  $J^k_{i\leftarrow j}$  between inter-residue atoms, i and j, can be evaluated as  $J^k_{i\leftarrow j}=\frac{1}{2}(\boldsymbol{v}_i\cdot\boldsymbol{F}_{ij}-\boldsymbol{v}_j\cdot\boldsymbol{F}_{ji})$  for trajectory k, where  $\boldsymbol{v}$  and  $\boldsymbol{F}$  are the velocity and the force of one atom on the other. The energy flux between residue pairs is computed as  $J^k_{A\leftarrow B}(t)=\sum_{i\in A}^{N_A}\sum_{j\in B}J^k_{i\leftarrow j}(t)$ , where  $N_A$  and  $N_B$  are the number of atoms in residues A and B, respectively. The energy current,  $L^k_{AB}=\frac{1}{RT}\lim_{t\to\infty}\int_0^{\tau}\langle J^k_{A\leftarrow B}(t_0)J^k_{A\leftarrow B}(t+t_0)\rangle dt$ , is computed, and the results are averaged. T is temperature, and R is the gas constant. Finally,  $G_{AB}$ , is the product of  $L_{AB}$  and RT,  $G_{AB}=(RT)L_{AB}$ , which has units (kcal mol $^{-1}$ ) $^2$  ps $^{-1}$ . In the following, the subscripts AB are dropped.

A focus of this study is the estimation of entropy change associated with the change in equilibrium fluctuations in the length of non-covalent contacts of  $\beta_2AR$  during activation, which is further related to change in G upon activation. We investigated changes in the dynamics of non-covalent contacts that can be categorized as polar, nonpolar, and charged. A contact is defined as polar where AH···O, A is oxygen or nitrogen, and the H···O distance is less than 2.8 Å and the polar contact is a hydrogen bond if the angle of AHO ≥150°. A polar contact is only included in the analysis if it is intact 99% of the time during the time G is computed. From the same trajectory, the length of a polar contact, r, and variance of the length of the contact  $\langle \delta r^2 \rangle = \langle (r - \langle r \rangle)^2 \rangle$  are computed and paired with the respective G. Furthermore, the contacts with -NH<sub>3</sub><sup>+</sup> and COO are grouped as charged. For the charged contacts considered here, we look only at hydrogen-bonded contacts between charged groups. To highlight sizable changes in G, a threshold of  $\Delta G > 50$  (kcal mol<sup>-1</sup>)<sup>2</sup> ps<sup>-1</sup> was employed for polar and charged contacts, and for nonpolar contacts, for which G is typically smaller, we used  $\Delta G > 5$  (kcal mol<sup>-1</sup>)<sup>2</sup> ps<sup>-1</sup>. It is helpful for clarity to bin data by averaging values of G for a range of  $\langle \delta r^2 \rangle^{-1}$ . Equidistant bin sizes of 584, 468, and 302 nm<sup>-2</sup> have been used for data plotted for polar, charged, and nonpolar contacts, respectively.

We evaluated nonpolar contacts if the average minimum distance, r, computed between two atoms of nonpolar groups was found to be less than 5.0 Å. In this case, the variance in the distance,  $\langle \delta r^2 \rangle = \langle (r - \langle r \rangle)^2 \rangle$ , was computed. If, e.g., a pair of phenylalanines satisfied the criterion of the average minimum distance between atoms of the side chains over 99% of the trajectory used to compute G, we compared the inverse variance of their minimum distances over time and paired with G.

## B. Energy transfer across $\beta_2AR$ contacts and relationship to contact dynamics and entropy

We consider the relationship between the energy current, G, across a non-covalent contact, which is proportional to the rate of energy transfer, and the variance in the length of the contact,  $(\delta r^2)^{-1}$ . We have argued<sup>38,40</sup> and shown in earlier work<sup>17,36,39</sup> that for many polar and non-polar contacts, they are related as  $G \propto (\delta r^2)^{-1}$ . A brief summary of that argument, based on harmonic models, is as follows: Consider a master equation for energy transfer between residue pairs in the protein,  $dE_A/dt = \sum_{A' \neq A} w_{AA'} E_{A'}$  $-w_{A'A}E_A$ , where  $E_A$  is the energy of residue A and  $w_{AA'}$ , a rate constant for residues A and A', is proportional to G. This equation appears similar to the equation of motion for lattice vibrations,  $m_A(d^2u_A/dt^2) = \sum_{A' \neq A} f_{AA'} u_{A'}$ , where  $m_A$  and  $u_A$  are the mass and displacement, respectively, at site A, and  $f_{AA'}$  is the spring constant. The two equations differ by the presence of a first-order time derivative in the master equation and second-order time derivative in the equation of motion for lattice vibrations. Some solutions to the master equation can be obtained from solutions to the vibrational dynamics by substituting t for  $\omega^{-2}$ ,  $z^{2,72-75}$  as has been found in computational studies of vibrational dynamics and energy flow in proteins. 61,76-78 For an oscillator,  $\omega^2 \propto (\delta r^2)^{-1}$ , so that for a rate,  $G \propto (\delta r^2)^{-1}$  after making the  $\omega^2$  to  $t^{-1}$  substitution. Small force constants are associated with lower frequencies and slower rates, and we expect energy transfer across nonpolar contacts to be slower than across polar contacts. The same proportionality has also been derived, again in harmonic approximation, using a different approach by Stock and co-workers.<sup>79</sup> Although protein dynamics is of course anharmonic, we have found  $G \propto \langle \delta r^2 \rangle^{-1}$  for many polar and nonpolar contacts from the results of MD simulations at 300 K.

If a given type of contact, such as a polar or van der Waals contact, follows  $G \propto (\delta r^2)^{-1}$  with the same constant of proportionality, we can estimate the change in dynamics and associated entropy when information about the change in the rate of energy transfer during the transition from one state to another is measured. At a fixed temperature, the change in entropy,  $\Delta S = S_2 - S_1$ , associated with the change in dynamics of the non-covalent contact going from states 1 to 2, with the change in force constant from  $f_1$  to  $f_2$  to be  $\Delta S = \frac{k_B}{2} \ln \left( \frac{f_1}{f_2} \right) = k_B \ln \left( \frac{\omega_1}{\omega_2} \right)$  in harmonic approximation. If  $G_1$  and  $G_2$  are proportional to the rate of energy transfer across a non-covalent contact of the inactive and active state, respectively, then, substituting  $t^{-1}$  for  $\omega^2$ , the change in entropy upon activation associated with a change in the dynamics of the contact is given by  $^{38,40}$ 

$$\Delta S = \frac{k_B}{2} \ln \left( \frac{G_1}{G_2} \right). \tag{1}$$

If the rate of vibrational energy transfer across the contact can be measured prior to and following activation, change in entropy associated with the dynamics of that contact can be determined. 38,40

We assume in Eq. (1) that the contact remains intact during activation. In practice, contacts will break and reform. We consider contacts that remain intact at least 50% of the simulation time in

both states. If  $x_i$  is the fraction of time the contact is intact in the inactive state, we, therefore, take  $G_1$  to be G that is computed for the residue pair in the inactive state divided by  $x_i$ . We are assuming that during the time the contact is broken, the value of G for the residue pair is comparatively small and can be neglected, so that  $G/x_i$  for that residue pair represents the energy current during the time the contact is intact in the inactive state. We do the same for the active state to obtain  $G_2$ .

### C. Estimate of change in entropy with change in protein volume

We can derive<sup>43</sup> a simple estimate to change in entropy for a small change in volume, V, in terms of the mode Grüneisen parameter,  $\gamma_{\alpha}$ , for a mode of frequency  $\omega_{\alpha}$ , defined as <sup>80–82</sup>

$$\gamma_{\alpha} = -\frac{V}{\omega_{\alpha}} \frac{\partial \omega_{\alpha}}{\partial V}.$$
 (2)

At constant temperature,

$$\left(\frac{\partial S_{\alpha}}{\partial V}\right) = \frac{C_{\alpha}\gamma_{\alpha}}{V},\tag{3}$$

where  $C_{\alpha}$  is the mode heat capacity for mode  $\alpha$ . If the volume changes from  $V_1$  to  $V_2$  at constant temperature, and the volume change is sufficiently small that we can neglect the change in  $C_{\alpha}$  with volume, an assumption supported by previous calculations, the change in entropy of mode  $\alpha$  is

$$\Delta S_{\alpha} = \gamma_{\alpha} C_{\alpha} \ln \left( \frac{V_2}{V_1} \right). \tag{4}$$

The thermal Grüneisen parameter,  $\gamma$ , is defined as <sup>80–82</sup>

$$\gamma = \frac{\sum_{\alpha} C_{\alpha} \gamma_{\alpha}}{\sum_{\alpha} C_{\alpha}},\tag{5}$$

where the sum is over all modes. If C is the sum of mode heat capacities over all modes,  $C = \sum_{\alpha} C_{\alpha}$ , the entropy change of the molecule with the change in volume is<sup>43</sup>

$$\Delta S = \gamma C \ln \left( \frac{V_2}{V_1} \right). \tag{6}$$

This estimate does not account for anisotropy in volume change. Nevertheless, we have obtained using Eq. (6) values similar to entropy change obtained using normal mode analysis and molecular dynamics simulations for several heme proteins.<sup>43</sup>

#### III. RESULTS AND DISCUSSION

#### A. Protein volume

When  $\beta_2AR$  becomes activated by an agonist, structural changes occur that include some opening in the cytoplasmic region, as illustrated in Fig. 1. The active state has been reported to be generally more flexible than the inactive state, particularly for the inactive state with an antagonist bound to it.<sup>8</sup> In Fig. 1, we superpose

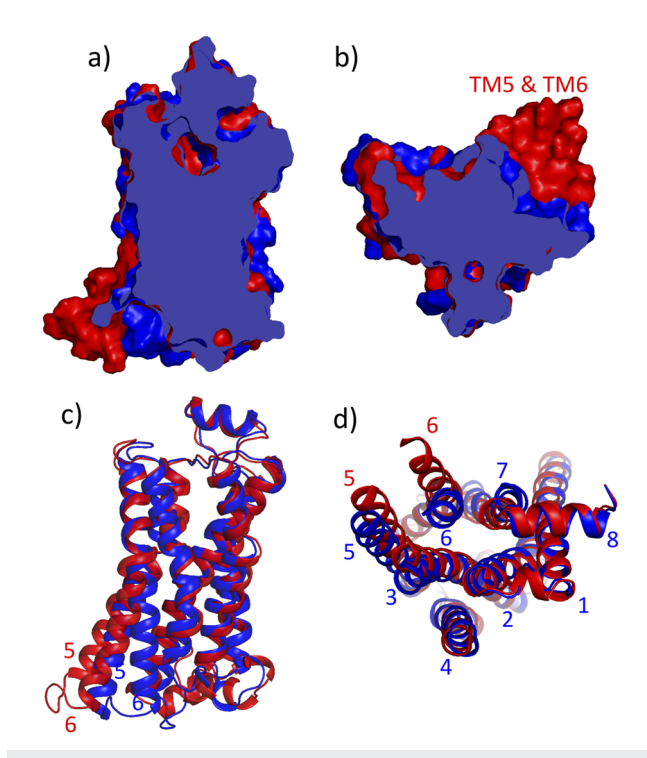


**FIG. 1.** Overlay of the active state (red) and inactive state (blue) of  $\beta_2AR$ . Cuts through the surface from the middle of the protein are shown (a) from a side view and (b) from the middle toward the cytoplasm. A significant contribution to the difference in volume is due to the opening of transmembrane helices (TM5 and TM6), shown from (c) a side view and (d) a cytoplasmic view. All transmembrane helices are labeled as is helix 8, which is in the cytoplasm.

inactive and active state structures to highlight some of the differences in protein volume, which appears overall slightly larger for the active state, particularly near the cytoplasm.

We use Protein Volume<sup>55</sup> to estimate the volume of  $\beta_2AR$  in inactive and active states. In Table I, we list average volumes computed for 20 structures sampled during the simulation. Since antagonist and agonist ligands are of different size, we compare volumes without the ligand. The average volume for the inactive state is 38 931 and 39 109 ų for the active state, so the volume is about 0.5% larger for the active state. The difference is attributed to the larger void volume of the active state, also listed in Table I. There are significant fluctuations in volume, particularly in the more flexible active state. The standard deviation in the volume is 85 and 209 ų for inactive and active states, respectively, due to fluctuations in the void volume.

The slightly larger average volume and lower packing density of the active state are consistent with its greater flexibility. We can estimate the change in entropy with change in volume using Eq. (6), which expresses entropy change in terms of mode Grüneisen parameters. We have previously computed mode Grüneisen parameters for myoglobin and computed  $\gamma C$  to be 10.435 kJ mol $^{-1}$  K $^{-1}$ . $^{43}$  Although the value can be somewhat different for different proteins,  $^{43}$  we use it to estimate  $\Delta S$  for activation of  $\beta_2 AR$ . Using the average protein volumes listed in Table I, we obtain

**TABLE I.** Average volumes of  $\beta_2AR$  computed for 20 structures during the MD simulations. Void volumes and van der Waals (vdW) volumes are also listed.

$\beta_2 AR$	Total volume (ų)	Void volume (ų)	vdW volume (ų)
Inactive (with antagonist)	39 411	9 845	29 566
Inactive (without antagonist)	38 931	9 643	29 288
Active (with agonist)	39 730	10 090	29 640
Active (without agonist)	39 109	9 808	29 301

 $\Delta S = 47.6 \text{ J mol}^{-1} \text{ K}^{-1}$ , a contribution of  $-14.3 \text{ kJ mol}^{-1}$  to the free energy of activation at 300 K.

This estimate should be seen as commensurate with the change to a slightly lower packing density for the transition to the active state. There are of course other contributions to the entropy change associated with the activation of the protein, including the number and nature of the transmembrane water molecules, which may be more tightly bound in the active state than the inactive state, as suggested by other studies of GPCR transmembrane water. <sup>18,22,83</sup> We consider now local contributions to entropy change.

## B. Rates of energy transfer and the relationship to dynamics of non-covalent contacts

We have found for many non-covalent contacts that the rate of energy transfer across the contact, which is proportional to G defined in Sec. II, is inversely proportional to the variance in the length of the contact, i.e.,  $G \propto \left\langle \delta r^2 \right\rangle^{-1}$ . We will see that this relationship holds well for contacts of  $\beta_2 AR$  that are largely intact in both the inactive and active states during the simulations, and for which there is a significant change in G during activation, as described in Sec. II. We find that for most of these contacts in the same class, i.e., polar, nonpolar, or charged, the constant of proportionality between G and  $\left\langle \delta r^2 \right\rangle^{-1}$  appears to be about the same.

Consider first the polar contacts of  $\beta_2AR$ . In Fig. 2, we plot  $G \propto \langle \delta r^2 \rangle^{-1}$  for polar contacts that remain intact at least 50% of the simulation time in both inactive and active states. We first summarize the main results and then provide more information about the trends observed in the data. In Fig. 2(a), we see that the data plotted for the contacts indicated in the figure fit reasonably well along a line, and a linear fit to the data is also shown in the figure. For clarity, we also bin the data, where we see the result (circles) to lie just along the linear fit to all the data. A linear fit to the binned data is almost identical to the linear fit to all data. We notice, however, that for one contact, Phe138-Gln142, the data for the inactive state and active state all appear to have similar  $\langle \delta r^2 \rangle^{-1}$  and thus do not fit the trend of the others. The reason for the anomalous behavior of Phe138-Gln142 will be discussed later. We, therefore, omit this contact and plot the results for all the polar contacts in Fig. 2(b). In Fig. 2(c), we compare with results for polar contacts of other proteins where the results appear similar. In Fig. 2(c), we also add results for hydrogen bonds between charged groups, which exhibit larger G at a particular  $(\delta r^2)^{-1}$ . The location of polar and charged contacts appears in Fig. 2(d).

We now discuss the results in more detail. In Fig. 2(a), all polar contacts of  $\beta_2AR$  that meet the criteria for remaining intact detailed

in Sec. II and for which the change in G is sufficiently large are plotted in both inactive and active states. The data for a particular contact are shown using the same color, where (+) indicates the inactive state and (•) indicates the active state. The linear fit to all the data (red line) is given by  $G = 0.015(\delta r^2)^{-1} + 8.6$  with an  $R^2$  value of 0.58. For clarity, we smoothed the data by averaging G in equidistant  $(\delta r^2)^{-1}$  bins as summarized in Sec. II. A linear fit to the binned data (open circles) for the polar contacts of  $\beta_2AR$  is given by  $G = 0.014(\delta r^2)^{-1} + 15.4$  with an  $R^2$  value of 0.97.

We see that the contact Phe138-Gln142 does not follow the trend of the other polar contacts, as the values of G for the active state are generally larger than for the inactive state, but the fluctuations in the length of the contact are similar in both states. The explanation for this anomaly is discussed below. We, therefore, remove the Phe138-Gln142 data in Fig. 2(b). The linear fit to the data (red line) is  $G = 0.016 \langle \delta r^2 \rangle^{-1} + 4.8$  with an  $R^2$  value of 0.66. We again bin for clarity and obtain as the linear fit to the binned data  $G = 0.015 \langle \delta r^2 \rangle^{-1} + 4.3$  with an  $R^2$  value of 0.98. The linear fits to the raw and binned data in Fig. 2(b) are essentially the same and they approach the origin, as is expected for the proportionality of G and  $\langle \delta r^2 \rangle^{-1}$ . The binned data are also plotted in Fig. 2(c), where they are compared with data for some of the polar contacts of HP36<sup>39</sup> and for some of the polar contacts of GLP-1R<sup>83</sup> computed previously.

Contacts involving charged groups exhibit typically larger G for a given variance in contact length and can follow different trends than those found for polar contacts.  $^{17,39,40}$  We plot results for hydrogen bonds between charged groups that remain intact in Fig. 2(c) and show the specific contacts that are plotted in Fig. 2(d). For these contacts, plotted in orange (binned data), of  $\beta_2AR$ , we obtain the linear fit  $G=0.030\langle\delta r^2\rangle^{-1}+46.1$  with a  $R^2$  value of 0.84. It turns out that this fit is close to the one we obtained for hydrogen bonds between charged groups of GLP-1R,  $^{83}$  a class B GPCR, for which we found the fit  $G=0.029\langle\delta r^2\rangle^{-1}+41.6$ , also shown in Fig. 2(c).

Overall, the polar contacts of two different classes of membrane-bound proteins and for HP36 exhibit the same linear trends indicating the same proportionality for  $G \propto \langle \delta r^2 \rangle^{-1}$ . For  $\beta_2 AR$ , the intact polar contacts are Thr136-171, Phe138-Gln142, Ala172-Ser176, Ile186-Val190, Trp77-Trp81, Ser176-Ser179, and Met187-Tyr191. Of the seven contacts identified, six are backbone–backbone interactions and Thr136-Tyr171 is a backbone-sidechain interaction. Many of these contacts, shown in Fig. 2(d), are at the edge of helices, which is also the case for the contacts of GLP-1R that are plotted in Fig. 2(c). Representation of the seven contacts might explain why the trends are so similar. The

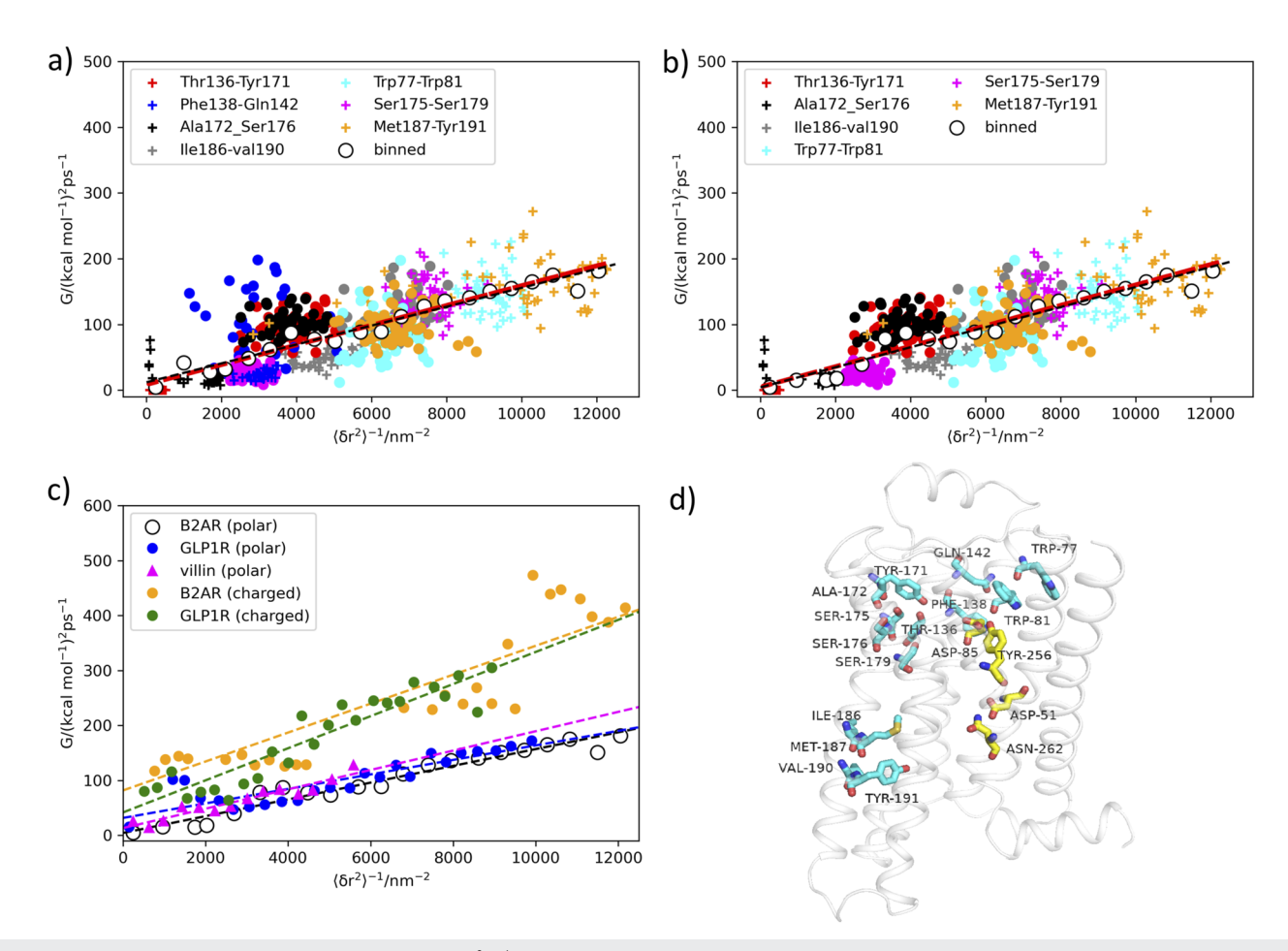


FIG. 2. (a) Plot of *G* vs inverse variance in contact length,  $(\delta r^2)^{-1}$ , for polar contacts of  $β_2AR$ , where (+) indicates inactive state and (•) active state, and the same color is used for a contact in both states. The legend indicates the color corresponding to a residue pair for both inactive and active states. The red line is a linear fit to the data and black line a linear fit to the binned data (open circles). (b) Same as (a) but data for Phe138-Gln142 removed (see text). (c) Comparison between the results of current and prior studies for polar contacts (lower trends) and hydrogen bonds between charged contacts (upper trends) of different proteins. Data for polar contacts of  $β_2AR$  (open circles), HP36<sup>39</sup> (magenta), and GLP-1R<sup>83</sup> (blue) yield similar trends. Data for hydrogen bonds between charged groups of  $β_2AR$  (orange) and GLP-1R<sup>83</sup> (green) also follow similar trends. (d) Location of the polar (cyan) and charged (yellow) contacts of  $β_2AR$ .

data for HP36 that are plotted correspond to polar contacts along helices.

In Table S2, we list the average value of G obtained for each of the contacts plotted in Fig. 2 in active and inactive states. We also list the fraction of time that the contact is found intact, and we use Eq. (1) to estimate the change in entropy associated with the change in dynamics in terms of the values of G that are computed for the contact in inactive and active states. For most of the contacts, the change in entropy associated with the change in dynamics is estimated between -6.5 and 6.5 J mol $^{-1}$  K $^{-1}$ , corresponding to a contribution of between -2 and 2 kJ mol $^{-1}$  to the free energy at 300 K. There is one exception, Thr136-Tyr179, for which we estimate  $\Delta S \approx -21$  J mol $^{-1}$  K $^{-1}$ . The reason for this very large change, discussed further below, is a freer motion in the inactive state of the tyrosine side chain that hydrogen bonds to the threonine backbone.

Consider now nonpolar (van der Waals) contacts. Rates of energy transfer across nonpolar contacts are typically smaller than across polar and charged contacts, but relatively small changes in G can correspond to a significant change in fluctuations in the length of the contact and corresponding entropy change, as estimated with Eq. (1). We find 14 nonpolar contacts to remain intact for the transition from inactive to active state based on the criteria in Sec. II. In Fig. 3, we plot G vs  $(\delta r^2)^{-1}$  for six of the 14 contacts.

We plot the intact nonpolar contacts exhibiting the largest (or smallest)  $G_{inactive}/G_{active}$  ratio among all the intact nonpolar contacts, since they are spread most in G and make the largest contribution to Eq. (1). Data for all intact nonpolar contacts are plotted in Fig. S5. Apart from one contact, Phe43-Val98, the data, both in Fig. 3 and in Fig. S5, appear to fall along the same trendline. Omitting the data for Phe43-Val98, the linear fit to the rest of the data in Fig. 3(a), plotted as the cyan line, is given by  $G = 0.0018(\delta r^2)^{-1} + 0.64$ , with

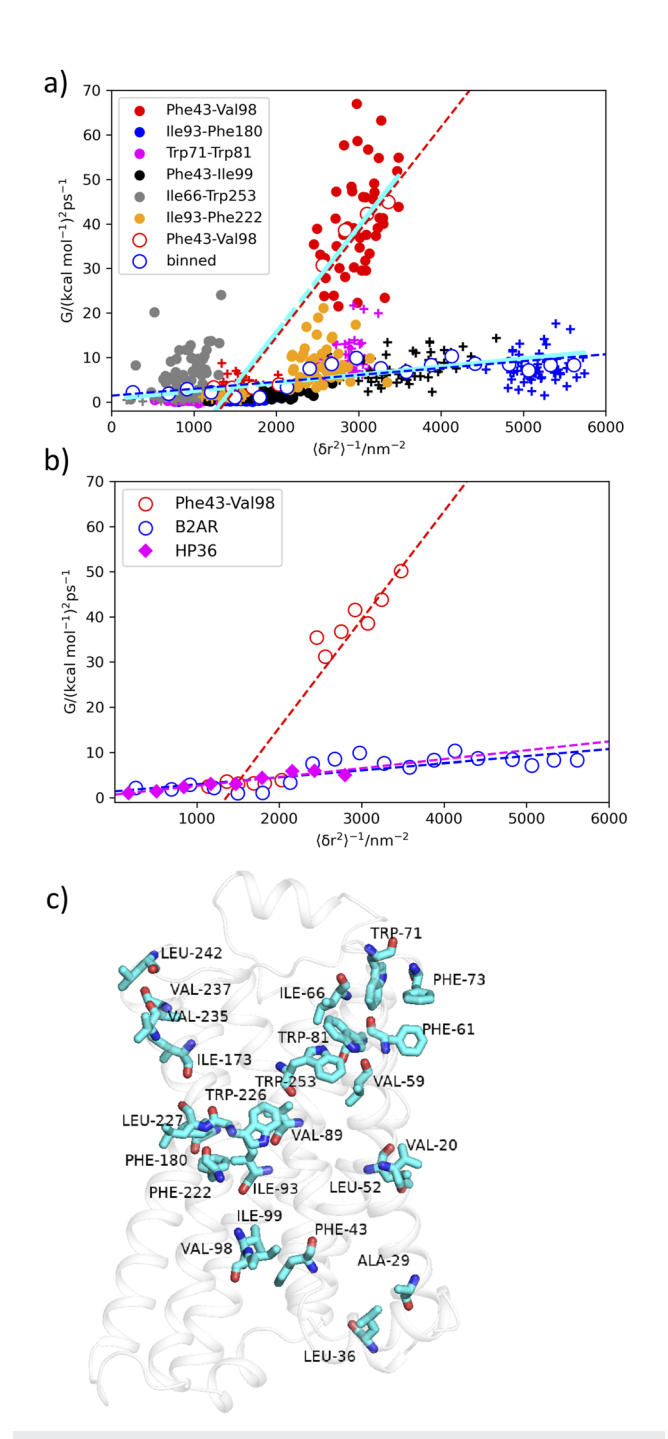


**FIG. 3.** (a) Plot of G vs inverse of the variance in contact length,  $(\delta r^2)^{-1}$ , for six nonpolar contacts of  $\beta_2 AR$ , where (+) indicates inactive state and (•) active state, and the same color is used for a contact in both states. The legend indicates the color corresponding to a residue pair for both inactive and active states. Open circles correspond to binned data, red for Phe43-Val98 and blue for all other contacts. The cyan line is a linear fit to all the data apart from Phe43-Val98, and the blue line a linear fit to the binned data (blue open circles). Data for Phe43-Val98 are shown separately in red (see text). (b) Comparison of binned data for nonpolar contacts of  $\beta_2 AR$  with binned data for nonpolar contacts of HP36. $^{39}$  (c) Location of all intact nonpolar contacts.

a  $R^2$  value of 0.31. For clarity, we have also binned the data, and a linear fit to the binned data is given by  $G=0.0015\langle\delta r^2\rangle^{-1}+1.42$  with a  $R^2$  value of 0.79. The linear fits are similar, and both appear to extrapolate close to the origin, as expected. The contact that is the exception to this trend, Phe43-Val98, is fitted separately to  $G=0.023\langle\delta r^2\rangle^{-1}-31.9$  with a  $R^2$  value of 0.84, a line that is also plotted in Fig. 3(a). The binned data of the contact Phe43-Val98 fits to  $G=0.023\langle\delta r^2\rangle^{-1}-32.7$  with a  $R^2$  value of 0.95 and is also plotted. We examine below the reason Phe43-Val98 does not fit the trend. In Fig. 3(b), the results for nonpolar contacts of  $\beta_2$ AR are compared with the results of nonpolar contacts of HP36, 39 where close agreement is found. The locations of all intact nonpolar contacts of  $\beta_2$ AR plotted are shown in Fig. 3(c).

We estimate the change in entropy associated with the change in dynamics of the contacts in terms of values of G for inactive and active states with Eq. (1). Values of G are listed in Table S3, where corresponding values of  $\Delta S$  are also listed. In Fig. 3, we have plotted the data for the contacts corresponding to the largest estimates for  $|\Delta S|$  and the other contacts listed follow the same trend except for Phe43-Val98, as noted. For the 13 contacts that are listed and for which we can use Eq. (1) to estimate  $\Delta S$ , the change in entropy associated with the change in dynamics is estimated between -7 and 11 J mol<sup>-1</sup> K<sup>-1</sup>, corresponding to a contribution of between -2.1 and 3.3 kJ mol<sup>-1</sup> to the free energy at 300 K. We find nine of the 13 nonpolar contacts to exhibit a positive change in entropy corresponding to greater flexibility in the active state. Including the seven polar contacts and two contacts formed by hydrogen bonds between charged groups (Fig. 2 and Table S2), we find 12 of 21 contacts to exhibit greater flexibility in the active state with on average a change of 0.35 J mol<sup>-1</sup> K<sup>-1</sup> per contact. It should be noted, however, that although the contacts are spread throughout the protein [see Figs. 2(d) and 3(c)], there may be some correlation in the values for different contacts.

The nonpolar contacts that we have identified to remain intact and to exhibit sizable change in G between the two states do so to a larger extent than the polar contacts and the hydrogen bonds between charged groups that remain intact. This occurs even if values of G tend to be larger across charged and polar contacts and often contribute more to energy flow through  $\beta_2 AR.^{41}$  Many nonpolar contacts remain intact in both states, and the relative change in G can be quite large. The nonpolar contacts remain intact 89% of the time compared with 78% for the polar and hydrogen bonds between charged groups. We expect that the change in dynamics of the larger number of intact nonpolar contacts with the change in state makes a greater contribution to the change in entropy than the change in dynamics of the intact polar contacts.

We now examine some of the contacts that exhibit notable trends in Figs. 2 and 3. We discuss examples of polar and non-polar contacts that fit the relationship  $G \propto (\delta r^2)^{-1}$  well as well as exceptions to the relation. For the seven polar contacts plotted in Fig. 2(a), the data for six of them appear to vary as  $G \propto (\delta r^2)^{-1}$ . Of these six contacts, Thr136-Tyr171 exhibits the largest change in dynamics between inactive and active states, and, using Eq. (1), the correspondingly largest entropy change,  $\Delta S$ . Snapshots of this contact for active and inactive states appear in Figs. 4(a) and 4(b), respectively. The large change in dynamics, and correspondingly large change in the value of G, is found to be associated with different packing around the contact by nearby residues. In the figure,

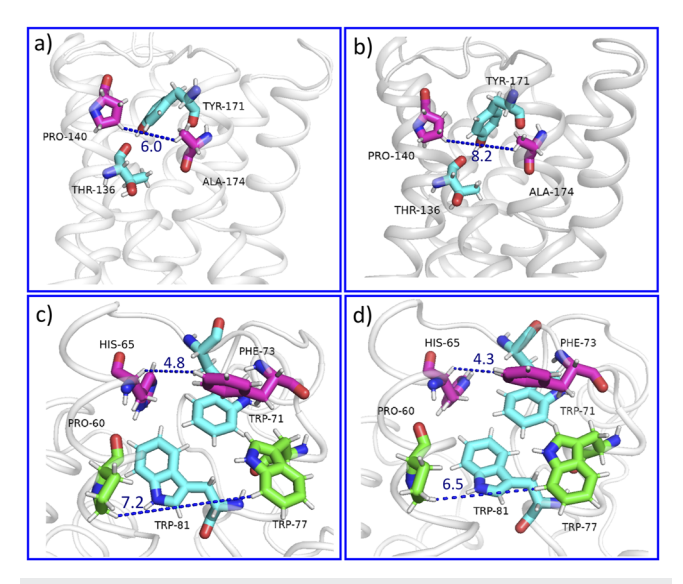


**FIG. 4.** Examples of polar and nonpolar contacts for which rates of energy transfer are described by the relation,  $G \propto (\delta r^2)^{-1}$  and which exhibit a relatively large change in G and  $(\delta r^2)^{-1}$  for the transition between inactive and active states. The polar contact Thr136-Tyr171 is shown in the (a) active and (b) inactive states. The average minimum distance between nearby residues Pro140 and Ala174 is smaller in the active state, restricting the motion of the Thr136-Tyr171 contact. The nonpolar contact Tyr71-Tyr81 in the (c) active state and (d) inactive state. The nearby residue pairs His65-Phe73 (magenta) and Pro60-Trp77 (green) and their average minimum distances are indicated.

the average minimum distance between the nearby residues Pro140 and Ala174 is indicated, computed to be 6.0 and 8.2 Å, respectively, in the active and inactive states. The proximity of Pro140 and Ala174 in the active state restricts the motion of Tyr171 in particular, resulting in a tighter contact with Thr136 and on average considerably larger G in the active state than the inactive state. Although the image shown is just one snapshot, clustering analysis of these residues was performed with a neighbor RMSD cutoff of 0.2 nm, and the structures fall within a single cluster (Fig. S1) containing the snapshots shown in Figs. 4(a) and (4b).

For all but one of the nonpolar contacts plotted in Fig. 3 and Fig. S5, the data exhibit the variation  $G \propto \langle \delta r^2 \rangle^{-1}$ . For example, data for the residue pair Tyr71-Tyr81 follow the trend and exhibit a large change in dynamics and G for the transition from inactive to active state. Snapshots of this contact are shown in Figs. 4(c) and 4(d) for the active and inactive states, respectively. As in the previous example, nearby residues appear to contribute to the change in dynamics of the contact, in this case, two pairs of them, His65-Phe73 and Pro60-Trp77, which are shown in magenta and green in both panels. The average minimum distance between His65 and Phe73 was computed during the MD simulations to be 4.8 Å in the active and 4.3 Å in the inactive state. The average minimum distance between Pro60 and Trp77 is 7.2 and 6.5 Å in the active and inactive state, respectively. Both pairs are closer to each other in the inactive state, restricting the motion of the Trp71-Trp81 contact, yielding a larger value of G. Clustering analysis indicates these residues fall within a single cluster oriented as in Figs. 4(c) and 4(d) (see Fig. S2). In these examples, where G and  $(\delta r^2)^{-1}$  both undergo sizable change with the transition between states, changes in the local environment with change in state contribute.

The data for one of the contacts plotted in Fig. 2 does not follow the trend  $G \propto \langle \delta r^2 \rangle^{-1}$ , and we now examine this case. For the residue pair Phe138-Gln142, we see in Fig. 2(a) that values of G, although quite different for the active and inactive states, cluster near similar values of  $(\delta r^2)^{-1}$ . We show a snapshot of Phe138-Gln142 in Figs. 5(a) and 5(b) for the active and inactive states, respectively. The orientation falls within a single cluster of the clustering analysis (Fig. S3). We observe in Fig. 5(a) a contact between the O atom of the side chain of Gln142 and the phenyl ring of Phe138, which we find 58% of the simulation time. This introduces a second contact between the residues, in addition to the hydrogen bond. For the inactive state, as shown in Fig. 5(b), the contact between the O-atom and the phenyl ring is found only 1% of the time. There is thus in the active state a second contact quite far from the hydrogen bond that is not found for the inactive state, giving rise to larger G with apparently little impact on dynamics of the hydrogen bonded

The data for one of the contacts plotted in Fig. 3, Phe43-Val98, also do not follow the trend  $G \propto (\delta r^2)^{-1}$ . Snapshots of the contact are shown in Figs. 5(c) and 5(d) for the active and inactive states, respectively. The orientation of these pairs remains the same in the simulations found within the same cluster in the clustering analysis (Fig. S4). In Fig. 5(c), we see multiple contacts between hydrogen atoms of Val98 and phenyl carbons of Phe43, for which the average distance is close to 3 Å. The average distance between three

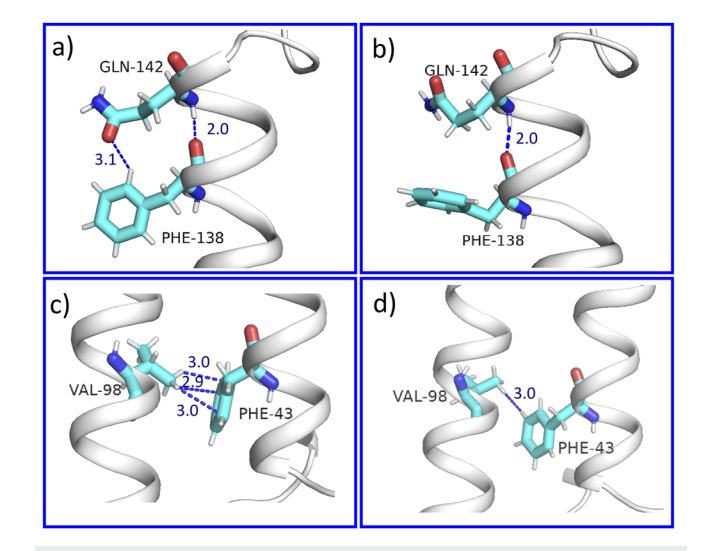


**FIG. 5.** Examples of polar and nonpolar contacts that do not exhibit the relationship  $G \propto \langle \delta r^2 \rangle^{-1}$ . Phe138-Gln142 in the (a) active and (b) inactive states. A second contact between the side chains is seen in the active state over most of the MD simulation while the contact is almost never found in the inactive state, affecting G but apparently not  $\langle \delta r^2 \rangle^{-1}$  for the hydrogen bonded contact at the backbone. Phe43-Val98 in the (c) active and (d) inactive states. Differences in the atoms forming the nonpolar contact due to the orientation of Val98 toward the phenyl ring of Phe43 yields a larger value of G in the active state with apparently only small change in  $\langle \delta r^2 \rangle^{-1}$ .

such contacts computed during the MD simulations is indicated. In Fig. 5(d), we see only one contact between Val95 and Phe43 that is comparable in distance. However, this contact is formed between two hydrogen atoms, while the average distance between the Val98 hydrogen to the nearest carbon of Phe43 is 4.8 Å. Thus, although there are contacts of similar length for both states that remain largely intact, they are of different nature, one between phenyl carbons and hydrogens of valine (active state) and the other between hydrogen atoms of the different residues (inactive). The different kinds of contacts apparently yield larger G in the active state without much difference in the fluctuations,  $(\delta r^2)^{-1}$ , of the contact length for the two states.

#### IV. CONCLUSIONS

We have examined some of the dynamic contributions to the activation of a GPCR,  $\beta_2AR$ , involved in allosteric regulation, with a focus on changes in the dynamics of non-covalent contacts during activation of  $\beta_2AR$  and the relationship to the rates of energy transfer across the contact. Rates of energy transfer across non-covalent contacts in proteins are currently being measured by time-resolved Raman and IR spectroscopies. <sup>27–35</sup> By relating rates of energy transfer to contact dynamics, the measurement of energy transfer rates across non-covalent contacts for different states of a protein can be interpreted in terms of changes in dynamics and associated entropy.

Active states of β<sub>2</sub>AR are generally more flexible than inactive states.8 We have estimated the change in volume of the protein for the transition from an antagonist-bound inactive to agonist-bound active state from the structures sampled during the MD simulations and find the volume of the active state to be on average slightly larger than the inactive state with a correspondingly lower packing density, consistent with greater flexibility. Using values of mode Grüneisen parameters computed for other proteins in the past, 43 we have estimated the change in entropy corresponding to the change in average volume, which, based on our calculations, is about 48 J mol<sup>-1</sup> K<sup>-</sup> for the transition from inactive to active state or a contribution of about -14 kJ mol<sup>-1</sup> to the free energy of activation at 300 K. Water is not included in this estimate. Interactions of GPCRs with water, including water in the transmembrane region, 18,22,83 change during activation and that effect needs to be accounted for as well, as activation is generally mediated by change in the dynamics of both protein and water. 15-17,84-92 Nevertheless, we see from this simple estimate the significance of dynamic contributions to allostery for a structured protein.

We have computed energy exchange networks (EENs), using the approach developed by Yamato and co-workers, <sup>45</sup> from the results of the MD simulations to identify contacts for which the rate of energy transfer changes with change in state of  $\beta_2AR$ . In earlier work, we related the change in the EEN to change in structure. <sup>41</sup> Here, we have reported changes in the EEN that are due to change in the dynamics of contacts. We have found more than 20 polar and nonpolar contacts that remain largely intact during activation and for which there is a significant change in the rate of energy transfer across the contact with a change in state. For all but two of those contacts, the rate of energy transfer across the contact varies inversely with the variance in the length of the contact.

Change in dynamics of polar and nonpolar contacts that remain largely intact during the transition from inactive to active state can be significant and corresponds to sizable change in entropy. The dynamic changes of almost all the contacts we have examined can be related to the change in rates of energy transfer across the contacts. We have examined some of the origins of the dynamic change, which can be due to a change in the orientation of nearby residues that interact with residues forming a particular contact, influencing their dynamics. We find many of the intact nonpolar contacts to exhibit sizable change in dynamics during activation, corresponding to a large relative change in the rate of energy transfer across the contact. Detecting changes in rates of energy transfer across nonpolar contacts may be more difficult than across polar contacts as the rates are usually significantly smaller. 36,39 Nevertheless, time-resolved Raman studies are providing information about energy flow between residues that interact by van der Waals forces.<sup>28–3</sup>

#### SUPPLEMENTARY MATERIAL

See the supplementary material for tables and figures with information about polar and nonpolar contacts, and clustering analysis.

#### **ACKNOWLEDGMENTS**

Support from NSF Grant No. CHE-1854271 was gratefully acknowledged. The authors were grateful to the Cyberinfrastructure Team in the Office of Information Technology at UNR for access to the Pronghorn HPC cluster, with allocation supported by UNR Student Technology Fees.

#### **AUTHOR DECLARATIONS**

#### **Conflict of Interest**

The authors have no conflicts to disclose.

#### **Author Contributions**

**Humanath Poudel**: Data curation (lead); Formal analysis (equal); Funding acquisition (supporting); Methodology (equal); Writing – original draft (equal); and Writing – review & editing (equal). **David M. Leitner**: Conceptualization (equal); Formal analysis (equal); Funding acquisition (lead); Methodology (equal); Writing – original draft (equal); and Writing – review & editing (equal).

#### **DATA AVAILABILITY**

The data that support the findings of this study are available from the corresponding author upon reasonable request.

#### **REFERENCES**

D. M. Leitner, C. Hyeon, and K. M. Reid, J. Chem. Phys. 152, 240901 (2020).
 O. Bozovic, C. Zanobini, A. Gulzar, B. Jankovic, D. Buhrke, M. Post, S. Wolf, G. Stock, and P. Hamm, Proc. Natl. Acad. Sci. U. S. A. 117, 26031–26039 (2020).
 P. I. Zhuralev and G. A. Papoian, Q. Rev. Biophys. 43, 295–332 (2010).

<sup>&</sup>lt;sup>4</sup>H. N. Motlagh, J. O. Wrabl, J. Li, and V. J. Hilser, Nature **508**, 331–339 (2014).

- <sup>5</sup>H. G. Saavedra, J. O. Wrabl, J. A. Anderson, J. Li, and V. J. Hilser, Nature **558**, 324–328 (2018).
- <sup>6</sup>Q. Cui and M. Karplus, Protein Sci. **17**, 1295–1307 (2008).
- <sup>7</sup>S.-R. Tzeng and C. G. Kalodimos, Nature **488**, 236–240 (2012).
- <sup>8</sup>W. I. Weis and B. K. Kobilka, Annu. Rev. Biochem. **87**, 897–919 (2018).
- <sup>9</sup>O. Miyashita, J. N. Onuchic, and P. G. Wolynes, Proc. Natl. Acad. Sci. U. S. A. **100**, 12570–12575 (2003).
- <sup>10</sup>O. Miyashita, P. G. Wolynes, and J. N. Onuchic, J. Phys. Chem. B **109**, 1959–1969 (2005).
- <sup>11</sup>M. Post, B. Lickert, G. Diez, S. Wolf, and G. Stock, J. Mol. Biol. 434, 167679 (2022).
- <sup>12</sup>D. Thirumalai, C. Hyeon, P. I. Zhuravlev, and G. H. Lorimer, Chem. Rev. **119**, 6788–6821 (2019).
- <sup>13</sup>E. Marcos, R. Crehuet, and I. Bahar, PLOS Comput. Biol. 7, e1002201 (2011).
- <sup>14</sup>R. Nussinov, C.-J. Tsai, and B. Ma, <u>Annu. Rev. Biophys.</u> **42**, 169–189 (2013).
- <sup>15</sup>S. Mondal and B. Bagchi, Curr. Opin. Struct. Biol. 77, 102462 (2022).
- <sup>16</sup>J. M. Laine, M. Amat, B. R. Morgan, W. E. Royer, and F. Massi, <u>Biochem</u> 53, 7199–7210 (2014).
- <sup>17</sup>K. M. Reid, T. Yamato, and D. M. Leitner, J. Phys. Chem. B **124**, 1148–1159 (2020).
- <sup>18</sup>Y. Lee, S. Kim, S. Choi, and C. Hyeon, *Biophys. J.* **111**, 1180–1191 (2016).
- $^{19}\,\mathrm{A.}$  Boffi and E. Chiancone, Methods Enzymol. 379, 55–64 (2004).
- <sup>20</sup> W. E. Royer, A. Pardanani, Q. H. Gibson, E. S. Peterson, and J. M. Friedman, Proc. Natl. Acad. Sci. U. S. A. **93**(12), 14526–14531 (1996).
- <sup>21</sup> P. Zhao, Y.-L. Liang, M. J. Belousoff, G. Deganutti, M. M. Fletcher, F. S. Willard, M. G. Bell, M. E. Christe, K. W. Sloop, A. Inoue, T. T. Truong, L. Clydesdale, S. G. B. Furness, A. Christopoulos, M.-W. Wang, L. J. Miller, C. A. Reynolds, R. Danev, P. M. Sexton, and D. Wootten, Nature 577, 432–436 (2020).
- <sup>22</sup> A. J. Venkatakrishnan, A. K. Ma, R. Fonseca, N. R. Latorraca, B. Kelly, R. M. Betz, C. Asawa, B. K. Kobilka, and R. O. Dror, Proc. Natl. Acad. Sci. U. S. A. 116(8), 3288–3293 (2019).
- <sup>23</sup> S. K. Huang, A. Pandey, D. P. Tran, N. L. Villanueva, A. Kitao, R. K. Sunahara, A. Sljoka, and R. S. Prosser, Cell **184**, 1884–1894 (2021).
- <sup>24</sup> A. J. Wand and K. A. Sharp, Annu. Rev. Biophys. **47**, 41–61 (2018).
- <sup>25</sup> V. Kasinath, K. A. Sharp, and A. J. Wand, J. Am. Chem. Soc. 135, 15092–15100 (2013).
- <sup>26</sup>J. A. Caro, K. W. Harpole, V. Kasinath, J. Lim, J. Granja, K. G. Valentine, K. A. Sharp, and A. J. Wand, Proc. Natl. Acad. Sci. U. S. A. 114, 6563–6568 (2017).
- <sup>27</sup> N. Fujii, M. Mizuno, H. Ishikawa, and Y. Mizutani, J. Phys. Chem. Lett. 5, 3269–3273 (2014).
- <sup>28</sup> M. Mizuno and Y. Mizutani, Biophys. Rev. **12**, 511–518 (2020).
- <sup>29</sup>Y. Mizutani, Bull. Chem. Soc. Jpn. **90**, 1344–1371 (2017).
- <sup>30</sup>S. Yamashita, M. Mizuno, and Y. Mizutani, J. Chem. Phys. **156**, 075101 (2022).
- <sup>31</sup>Y. Mizutani and M. Mizuno, "Time-resolved spectroscopic mapping of vibrational energy flow in proteins: Understanding thermal diffusion at the nanoscale," J. Chem. Phys. **157**, 240901 (2022).
- <sup>32</sup>T. Baumann, M. Hauf, F. Schildhauer, K. B. Eberl, P. M. Durkin, E. Deniz, J. G. Löffler, C. G. Acevedo-Rocha, J. Jaric, B. M. Martins, H. Dobbek, J. Bredenbeck, and N. Budisa, Angew. Chem. 58, 2899–2903 (2019).
- <sup>33</sup> E. Deniz, L. Valiño-Borau, J. G. Löffler, K. B. Eberl, A. Gulzar, S. Wolf, P. M. Durkin, R. Kaml, N. Budisa, G. Stock, and J. Bredenbeck, Nat. Commun. 12, 3284 (2021).
- <sup>34</sup>E. H. G. Backus, R. Bloem, R. Pfister, A. Moretto, M. Crisma, C. Toniolo, and P. Hamm, J. Phys. Chem. B **113**, 13405–13409 (2009).
- <sup>35</sup>J. G. Löffler, E. Deniz, C. Feid, V. G. Franz, and J. Bredenbeck, <u>Angew. Chem.</u> 134, e202200648 (2022).
- <sup>36</sup>S. Buchenberg, D. M. Leitner, and G. Stock, J. Phys. Chem. Lett. **7**, 25–30 (2016).
- <sup>37</sup>D. M. Leitner, S. Buchenberg, P. Brettel, and G. Stock, J. Chem. Phys. **142**, 075101 (2015).
- <sup>38</sup>D. M. Leitner, H. D. Pandey, and K. M. Reid, J. Phys. Chem. B **123**, 9507–9524 (2019).
- <sup>39</sup> H. Poudel, K. M. Reid, T. Yamato, and D. M. Leitner, J. Phys. Chem. B **124**, 9852–9861 (2020).

- <sup>40</sup> K. M. Reid, T. Yamato, and D. M. Leitner, J. Phys. Chem. B **122**(40), 9331–9339 (2018).
- <sup>41</sup> H. Poudel and D. M. Leitner, J. Phys. Chem. B 125(24), 6522–6531 (2021).
- <sup>42</sup> A. Cooper and D. T. F. Dryden, Eur. Biophys. J. **11**, 103–109 (1984).
- <sup>43</sup> K. M. Reid, X. Yu, and D. M. Leitner, J. Chem. Phys. **154**, 055012 (2021).
- <sup>44</sup>S. G. F. Rasmussen, B. T. Devree, Y. Zou, A. C. Kruse, K. Y. Chung, T. S. Kobilka, F. S. Thian, P. S. Chae, E. Pardon, D. Calinski, J. M. Mathiesen, S. T. A. Shah, J. A. Lyons, M. Caffrey, S. H. Gellman, J. Steyaert, G. Skiniotis, W. I. Weis, R. K. Sunahara, and B. K. Kobilka, Nature 477(7366), 549–557 (2011).
- <sup>45</sup>T. Ishikura, Y. Iwata, T. Hatano, and T. Yamato, J. Comput. Chem. 36(22), 1709–1718 (2015).
- <sup>46</sup>L. Di Paola, H. Poudel, M. Parise, A. Giuliani, and D. M. Leitner, Entropy 24, 998 (2022).
- <sup>47</sup>S. G. F. Rasmussen, H. J. Choi, J. J. Fung, E. Pardon, P. Casarosa, P. S. Chae, B. T. Devree, D. M. Rosenbaum, F. S. Thian, T. S. Kobilka, A. Schnapp, I. Konetzki, R. K. Sunahara, S. H. Gellman, A. Pautsch, J. Steyaert, W. I. Weis, and B. K. Kobilka, Nature 469 (7329), 175–181 (2011).
- <sup>48</sup>V. Cherezov, D. M. Rosenbaum, M. A. Hanson, S. G. F. Rasmussen, F. S. Thian, T. S. Kobilka, H.-J. Choi, P. Kuhn, W. I. Weis, B. K. Kobilka, and R. C. Stevens, Science 318, 1258–1265 (2007).
- <sup>49</sup> A. Fiser and A. Sali, <u>Bioinformatics</u> **19**, 2500–2501 (2003).
- $^{\bf 50}$  S. Jo, T. Kim, V. G. Iyer, and W. Im, J. Comput. Chem. **29**, 1859–1965 (2008).
- <sup>51</sup> P. Mark and L. Nilsson, J. Phys. Chem. A **105**, 9954–9960 (2001).
- <sup>52</sup>J. A. Maier, C. Martinez, K. Kasavajhala, L. Wickstrom, K. E. Hauser, and C. Simmerling, J. Chem. Theory Comput. 11(8), 3696–3713 (2015).
- <sup>53</sup> C. J. Dickson, B. D. Madej, Å. A. Skjevik, R. M. Betz, K. Teigen, I. R. Gould, and R. C. Walker, J. Chem. Theory Comput. 10, 865–879 (2014).
- <sup>54</sup> H. J. C. Berendsen, J. P. M. Postma, W. F. van Gunsteren, A. DiNola, and J. R. Haak, J. Chem. Phys. **81**(8), 3684–3690 (1984).
- <sup>55</sup>C. R. Chen and G. I. Makhatadze, <u>BMC Bioinf.</u> **16**, 101 (2015).
- <sup>56</sup>D. M. Leitner and J. E. Straub, *Proteins: Energy, Heat and Signal Flow* (CRC Press, Taylor and Francis Group, Boca Raton, FL, 2010).
- <sup>57</sup> H. Fujisaki and J. E. Straub, J. Phys. Chem. B 111, 12017–12023 (2007).
- <sup>58</sup>P. H. Nguyen, S. M. Park, and G. Stock, J. Chem. Phys. **132**, 025102 (2010).
- <sup>59</sup>Y. Xu and D. M. Leitner, J. Phys. Chem. B 118, 7818–7826 (2014).
- <sup>60</sup> J. K. Agbo, Y. Xu, P. Zhang, J. E. Straub, and D. M. Leitner, Theor. Chem. Acc. 133, 1504 (2014).
- <sup>61</sup> D. M. Leitner, Annu. Rev. Phys. Chem. **59**, 233–259 (2008).
- 62 S. Wu and A. Ma, J. Chem. Phys. 156, 054119 (2022).
- 63 W. Li and A. Ma, J. Chem. Phys. 144, 114103 (2016).
- <sup>64</sup> M. Nagaoka, I. Yu, and M. Takayanagi, in *Proteins: Energy, Heat and Signal Flow*, edited by D. M. Leitner and J. E. Straub (Taylor and Francis Group, CRC Press, Boca Raton, 2010), pp. 169–196.
- <sup>65</sup> M. Takayanagi, H. Okumura, and M. Nagaoka, J. Phys. Chem. B 111, 864–869 (2007).
- $^{66}\mathrm{C}.$  Chennubhotla and I. Bahar, PLOS Comput. Biol. 3, 1716–1726 (2007).
- <sup>67</sup>D. M. Leitner and T. Yamato, Biophys. Rev. **12**, 317–322 (2020).
- <sup>68</sup>N. Helmer, S. Wolf, and G. Stock, J. Phys. Chem. B **126**, 8735–8746 (2022).
- <sup>69</sup> K. Ota and T. Yamato, J. Phys. Chem. B **123**(4), 768–775 (2019).
- <sup>70</sup>T. Yamato, T. Wang, W. Sugiura, O. Laprevote, and T. Katagiri, J. Phys. Chem. B **126**, 3029–3036 (2022).
- $^{71}$  D. M. Leitner and T. Yamato, in *Reviews in Computational Chemistry*, edited by A. L. Parrill and K. B. Lipkowitz (John Wiley and Sons, Inc., 2018), Vol. 31, pp. 63–114.
- pp. 63–114. <sup>72</sup>T. Nakayama, Y. Kousuke, and R. L. Orbach, Rev. Mod. Phys. **66**, 381–443 (1994).
- 73 S. Alexander and R. Orbach, J. Phys. Lett. 43, L625–L631 (1982).
- <sup>74</sup>S. Alexander, J. Bernasconi, W. R. Scheider, and R. Orbach, Rev. Mod. Phys. **53**, 175–198 (1981).
- <sup>75</sup>R. Rammal and G. Toulouse, J. Phys. Lett. **44**, L13–L22 (1983).
- <sup>76</sup> X. Yu and D. M. Leitner, J. Chem. Phys. **119**, 12673–12679 (2003).
- <sup>77</sup> M. B. Enright, X. Yu, and D. M. Leitner, Phys. Rev. E 73, 051905 (2006).
- <sup>78</sup>M. B. Enright and D. M. Leitner, *Phys. Rev. E* **71**, 011912 (2005).
- <sup>79</sup>L. Valino-Borau, A. Gulzar, and G. Stock, J. Chem. Phys. **152**, 045103 (2020).

- <sup>80</sup> N. W. Ashcroft and N. D. Mermin, *Solid State Physics* (Holt, Rinehart and Winston, Philadelphia, 1976).
- <sup>81</sup> G. Dolling and R. A. Cowley, Proc. Phys. Soc. **88**, 463–494 (1966).
- <sup>82</sup>J. Fabian and P. B. Allen, *Phys. Rev. Lett.* **79**, 1885–1888 (1997).
- 83 H. Poudel and D. M. Leitner, J. Phys. Chem. B 42, 8362–8373 (2022).
- <sup>84</sup>X. Yu, J. Park, and D. M. Leitner, J. Phys. Chem. B **107**, 12820–12829 (2003).
- 85 H. D. Pandey and D. M. Leitner, J. Phys. Chem. B 121, 9498–9507 (2017).
- <sup>86</sup> K. M. Reid, A. K. Singh, C. R. Bikash, J. Wei, Y. Tal-Gan, N. Q. Vinh, and D. M. Leitner, Biophys. J. 121, 540–551 (2022).
- <sup>87</sup> M. Heyden, J. Chem. Phys. **150**, 094701 (2019).

- <sup>88</sup> A. Chowdhury, S. A. Kovalenko, I. V. Aramburu, P. S. Tan, N. P. Ernsting, and E. A. Lemke, Angew. Chem., Int. Ed. **58**, 4720–4724 (2019).
- <sup>89</sup> M.-C. Bellissent-Funel, A. Hassanali, M. Havenith, R. Henchman, P. Pohl, F. Sterpone, D. vanderSpoel, Y. Xu, and A. E. Garcia, Chem. Rev. **116**, 7673–7697 (2016).
- <sup>90</sup>H. Wirtz, S. Schäfer, C. Hoberg, K. M. Reid, D. M. Leitner, and M. Havenith, Biochem **57**, 3650–3657 (2018).
- <sup>91</sup> V. C. Nibali, S. Pezzotti, F. Sebastiani, D. R. Galimberti, G. Schwaab, M. Heyden, M. P. Gaigeot, and M. Havenith, J. Chem. Phys. Lett. 11, 4809–4816 (2020).
- <sup>92</sup>Y. Levy and J. N. Onuchic, Annu. Rev. Biophys. Biomol. Struct. 35, 389–415 (2005).